A Low-Cost Minimally-Processed Inkjet-Printed Nonlinear Element for Reservoir Computing

Shahrin Akter and Mohammad Rafiqul Haider
Dept. of Electrical Engineering and Computer Science
University of Missouri
Columbia, MO, U.S.A.
{shahrin.akter, mhaider}@missouri.edu

***Abstract*—In the realm of flexible substrate technology, inkjet printing has emerged as a highly sought-after method due to its cost-effectiveness, scalability for mass production, simplicity, and environmental sustainability. While recent advancements have led to the development of fully printed artificial neurons, realizing a fully printed Echo State Network (ESN) remains elusive. This study introduces a novel approach involving the fabrication of a low-cost, minimally processed, nonlinear computation element entirely through inkjet printing. Positioned on a polyethylene terephthalate film substrate, this element serves as the activation function for an Echo State Network. The conventional activation function within the ESN architecture is supplanted by the electrical response curve of the inkjet-printed neuron. This neuron is constructed using silver nanoparticle ink, complemented by a layer of hexagonal boron nitrade. To assess the activation performance for time series prediction within the Echo State Network framework, the Mackey-Glass time series data is employed as a benchmark. Comparative analysis is conducted against established conventional activation functions, utilizing test mean squared error as the performance metric. The outcomes of this evaluation highlight the efficacy of the proposed nonlinear computational element as an activation function within the Echo State Network paradigm.**

***Index Terms*—Activation function, Echo State Network, Inkjet-printed circuit, Reservoir computing.**

I. Introduction

Silicon-based technologies have been pivotal in the realm of high-speed digital processing, laying the groundwork for the evolution of electronics. Their contribution to the miniaturization and enhancement of electronic devices has been unparalleled, facilitating the creation of low-power sensing and signal processing [1]–[8], wireless powering [9]–[11], and high-performance computing systems [12], [13]. Yet, further venture into minimizing transistor sizes, in accordance with Moore's Law, is confronted by substantial physical constraints [14]. Innovative alternatives are being explored, including carbon nanotube-based electronics [15], memristor [16], quantum dot [17] and other non-conventional methods [18]–[20], all of which offer prospects that transcend the capabilities of conventional silicon-based devices and hold the potential to redefine our approach to computational processing power in the forthcoming era.

However, these nascent technologies face their own set of challenges, such as resource limitations, difficulties in transitioning from lab to market, environmental concerns, and cost constraints [21] [22]. Inkjet-printed electronics emerge as a solution to these limitations, boasting attributes that make them ideal for compact, energy-efficient, and cost-effective non-linear circuits that facilitate alternative computational processes [23]–[25]. Additionally, the versatility of inkjet printing technology allows deposition of electronic materials on a variety of substrates [26], including textiles and irregular surfaces. This low-cost and straightforward fabrication technique enables rapid prototyping and design iteration—a stark contrast to the lengthy fabrication cycles associated with CMOS technologies. For the past two decades, inkjet-printed circuits have played a crucial role in the development of sensors [27]–[29], antennas [30]–[32], and reservoir computing systems [33]. Inkjet-printed memristor created with this method, are proving to be comparable in function to their MOSFET counterparts fabricated with high-precision laboratory equipment [34]. This technique can be adeptly applied to construct physical neural networks by arranging multiple units in configurations compatible with echo state networks (ESN) [35], liquid state machines [36] other reservoir computing systems [37]. Previously, inkjet-printed memristive device is used to build a artificial neural neuron, which provides comparable result in ESN framework [38]. This inkjet-printed memristive device exhibits behavior characterized by a hyperbolic sine curve across a broad voltage spectrum, which results in increased power consumption. There is potential for research to minimize this voltage range, and this work aims to address this gap.

This paper presents an innovative inkjet-printed non-linear computation element with memristive response in a small voltage range, for developing low-power computing systems. Specifically, this study explores the utility of inkjet-printed memristive response within the ESN paradigm to predict benchmark Mackey-Glass time series signal. The structure of the paper is organized as follows: an overview of inkjet-printed technology, ESN architecture and activation function are provided in Section II, III and IV respectively. Proposed inkjet printed non-linear computation element is described in section V and followed by a comprehensive presentation of the electrical modeling in section VI. The design of ESN with a nonlinear computation element as an activation function is delineated in section VII and followed by the findings and extensive analysis in section VIII. The paper concludes by summarizing the study's conclusions in Section IX.

II. Inkjet-Printed Technology

In basic inkjet printing technology, there are primarily two essential steps: (1) designing the pattern using a digital editing tool and (2) printing the pattern onto a substrate using a compatible printer. To enhance the quality of the printing, additional fabrication steps such as substrate pre-processing, plasma treatment, and curing are incorporated. Depending on research requirements, novel materials like silver nanoparticles, graphene, hexagonal boron nitride (hBN) etc. are employed. Most inkjet printing systems utilize the Dimatix Material Printer (DMP) for printing purposes.

III. ESN Architecture

ESN, a type of reservoir computing, was introduced by Jaeger [35]. ESNs consist of three layers: an input layer, a reservoir, and an output layer, which is also referred to as the readout layer. Data is fed into the ESN through the input layer and transformed into a higher-dimensional space within the reservoir. The weights and biases of the input layer and reservoir are randomly assigned during the initial setup and remain fixed during training, making these layers non-trainable. The only trainable part of an ESN is the readout layer, where weights and biases are adjusted using simple learning algorithms like linear regression [39]. Fig. 1 illustrates the basic structure of an ESN. The dynamic laws governing the updates of the reservoir and output states are defined by equation (1) and (2) respectively.

$$x(n+1) = f(W_{in}u(n+1) + W_{res}x(n)) \tag{1}$$

$$y(n+1) = W_o x(n+1) \tag{2}$$

where,
u(n) = Input state vector
x(n) = Reservoir state vector
y(n) = Output state vector
W_{in} = Input weight matrix
W_{res} = Reservoir weight matrix
W_o = Output weight matrix
f(.) = Non-linear activation function

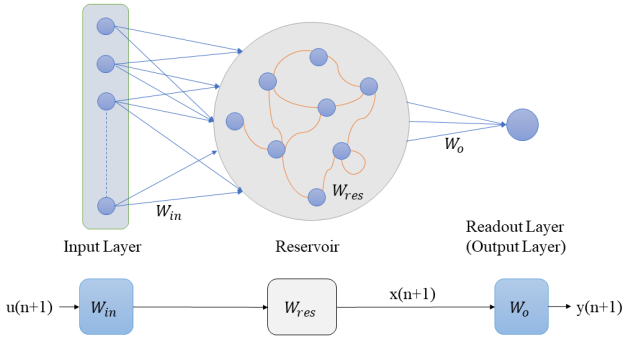

Fig. 1. Generic architecture of an ESN.

To ensure the echo state property in a reservoir's weight matrix, it is essential to scale the matrix by its spectral radius, denoted as λ_{max}. Typically, the reservoir is sparsely connected, with about 90-95% of the elements in the reservoir weight matrix being zero. The popularity of ESN is increasing due to their straightforward computational requirements and reduced processing time, making them well-suited for hardware implementations.

IV. Activation Function

Neural networks consist of units called artificial neurons, which non-linearly transform their inputs using mathematical functions known as activation or squashing functions. A single neuron alone cannot linearly separate input data; a network of neurons is required for effective data separation. Most commonly used activation functions include sigmoid, hyperbolic tangent (tanh), rectified linear unit (ReLU), and leaky ReLU, as shown in Fig. 2. Beyond these, there are additional variations of these functions.

The ReLU function provides the input values in outputs directly for positive input values; otherwise, it outputs zero. On the other hand, leaky ReLU, a variant of ReLU, allows a small, non-zero, output with smaller slope for negative inputs. The sigmoid function maps any input to a range between 0 and 1, while tanh provides output values between -1 and 1. A limitation of the standard tanh and sigmoid functions is their gradual transition from high to low values, which can obscure minor dynamic changes in input. Other variations, like the hyperbolic sine function, exhibit similar nonlinearities. The nonlinearity of the tanh function is somewhat analogous to the behavior of inkjet-printed computing systems, which exhibit a steeper slope and two pinch points in transitions. These aid in the detection of small dynamic changes in inputs, making them suitable for modeling inkjet-printed computing systems and for use in computer-based experimental setups.

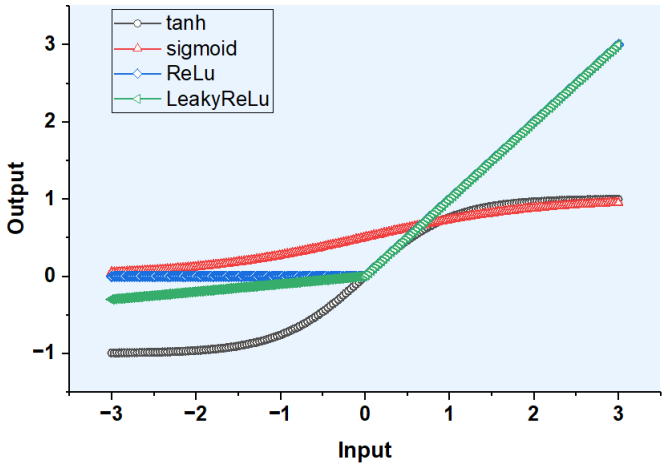

Fig. 2. Characteristics of most commonly used activation functions including hyperbolic tangent, sigmoid, ReLU, and Leaky ReLU.

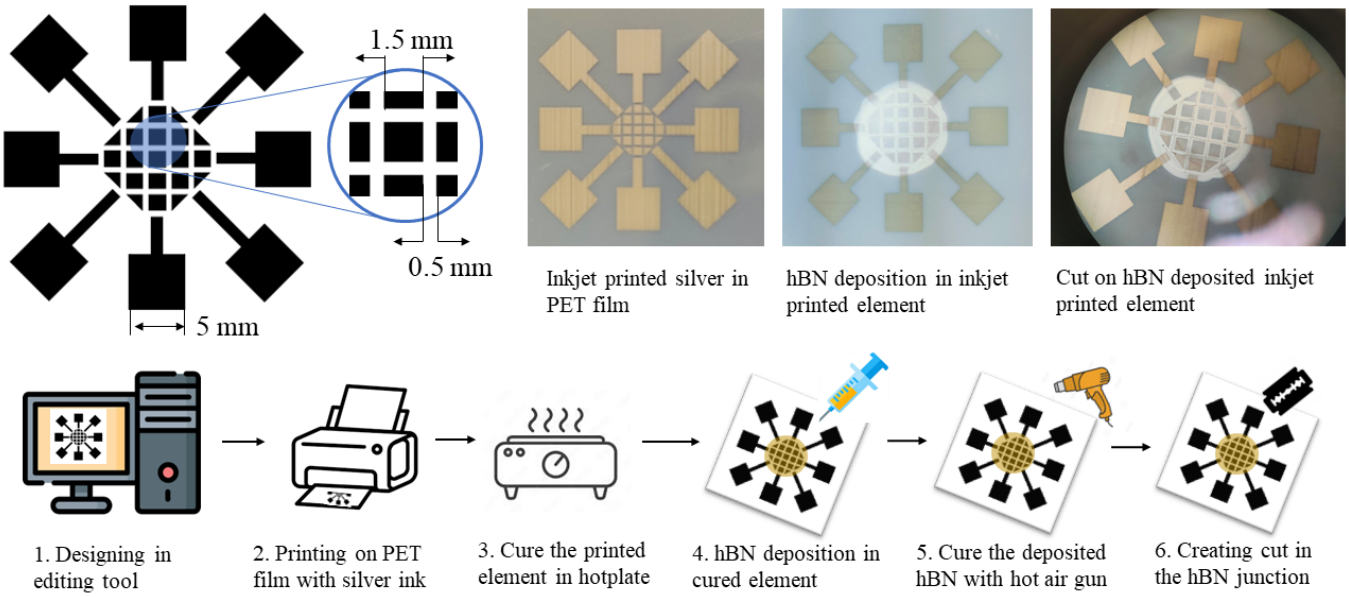

Fig. 3. Inkjet printed fabrication process of the nonlinear element is shown in the flowchart. Along with the flowchart, images of nonlinear elements in different steps are shown along with all relevant dimensions.

V. Proposed Inkjet-printed non-linear computation element

This study introduces a non-linear computing component created using inkjet printing technology. The component was initially designed using a graphic editing software and then transferred onto a 135 μm thick PET film using a drop-on-demand piezoelectric inkjet printer, which utilizes silver nanoparticle ink. The silver nanoparticle ink utilized in this study serves as a conductor for non-linear computing element and is formulated in a noncombustible, eco-friendly aqueous solution. It is non-toxic to humans and does not require sintering during the fabrication process. The nanoparticles have an approximate diameter of 20 nm, and the ink's viscosity is suitable for printing through inkjet printer nozzles. Following the printing process, the component underwent a curing phase on a hotplate for a specified duration.

Subsequently, a layer of hBN which works as dielectric was applied at the component's junction and then subjected to further curing with a hot air gun. The deposition of hBN was meticulously carried out using a precision pipette, although some variability in the thickness and uniformity of the deposited layers was noted, which is likely a consequence of manual handling. This material is used for insulating substrate which is essential for subsequent steps. The final step involved making a precise cut at the junction of the element. A significant challenge in the curing step of inkjet printing technology is the coffee-ring effect, which leads to the natural accumulation of high-concentration nanoparticles at the edges of the dried ink. This effect compromises nanoparticle uniformity, affecting the reliability and repeatability of samples. This issue is resolved by etching a well into the hBN across the gap. The flowchart in Fig. 3 illustrates the sequence of steps in the inkjet printing process and includes images of the component at various stages of fabrication process.

At the center of the non-linear element, there are 13 square blocks, each with 1.5 mm sides, arranged alongside 8 triangular blocks of the same length along two sides. The dimensions and shapes of these square blocks can be modified. All these shapes are evenly spaced, maintaining a 0.2 mm gap between them, a dimension influenced by the printer's resolution limit due to the sputtering effect in printing. From the central part of the non-linear element, eight connectors extend outward, each utilizing a square block that measures 5 mm in length to facilitate these connections. Fig. 3 details the specific dimensions of the non-linear computational element.

VI. Electrical design of non-linear computational element

I-V characteristics of the non-linear computational element were assessed using a Keithley 2604B Dual Channel Source Measure Unit. The unit conducted a voltage sweep from -5 volts to +5 volts and returned to -5 volts, a cycle which was repeated twice to confirm the stability of the current and to check for hysteresis effects. The resulting I-V curve for the inkjet-printed non-linear computational element is depicted in Fig. 4. This curve clearly demonstrates that within a narrow voltage range of [-1,1]V, the element undergoes a current transition within the range of [-0.8,0.8] nA. The reverse path of the hysteresis loop resembles the hyperbolic tangent function and features two pinch-off points during the transition. Current research indicates that the nonlinearity of the I-V profile is caused by hopping conduction in the silver nanoparticle ink, leading to its potential application in analog neural networks as mentioned in the literature [40].

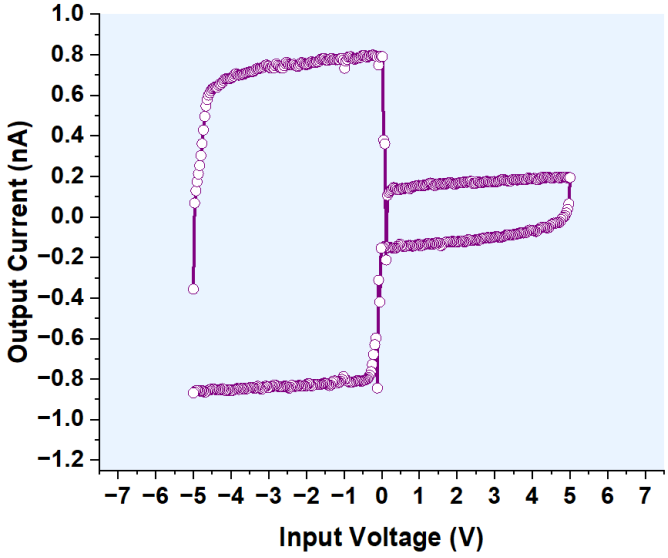

Fig. 4. I-V characteristics of the non-linear computational element. Voltage sweep of two cycles ensure the hysteresis properties of the element.

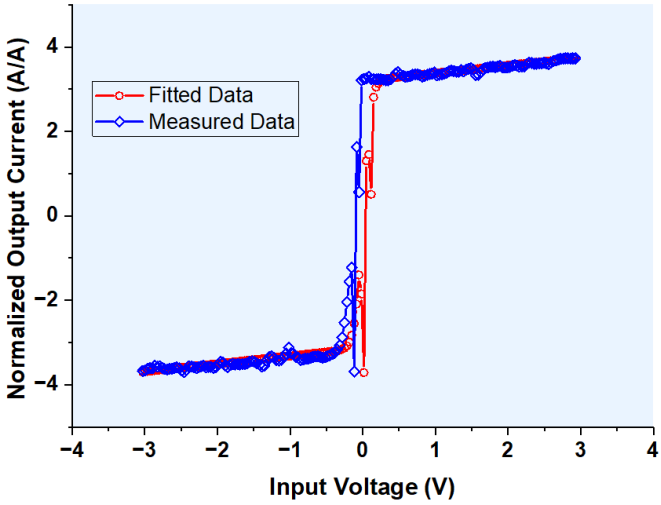

Fig. 5. I-V characteristics of the non-linear computation element and best-fitted activation function for ESN.

The observed backward I-V curve of the element could potentially serve as an activation function for neural networks, offering an alternative to the widely used hyperbolic tangent function. The unique pinch-off characteristics observed during the transition could yield enhanced sensitivity in that region. Fig. 5 presents the I-V characteristics of the non-linear element alongside the optimally fitted curve for the proposed custom activation function. To fit the custom activation function to the I-V characteristics of the non-linear element, mathematical tanh function is modified with some additional constant values to control the slope and position of the tanh function. Along with this, pinch off of the I-V curve is replicated in the custom activation function with Gaussian function, where position and spread of the pinch off is controlled by the mean and variance of the Gaussian function. Moreover, height of the pinch of is replicated by adding a factor in the Gaussian function. Custom activation function is defined by (3).

$$f(x) = t(x) \times g_1(x) \times g_2(x) \tag{3}$$

Where, t(x) is the modified tanh function, $g_1(x)$ and $g_2(x)$ are the gaussian functions to replicate pinch off in activation function.

$$t(x) = a \tanh(bx) + dx^2 + c \tag{4}$$

$$g_1(x) = \frac{h_1}{\sigma_1\sqrt{2\pi}} e^{-(x-\mu_1)^2/2\sigma_1^2} \tag{5}$$

$$g_2(x) = \frac{h_2}{\sigma_2\sqrt{2\pi}} e^{-(x-\mu_2)^2/2\sigma_2^2} \tag{6}$$

Here, constant a, b, c, d controls the position and slope of tanh function. μ_1, μ_2 mean of both gaussian functions control the position of pinch off, whereas, σ_1, σ_2 variance of gaussian function controls the width of pinch off and h_1, h_2 controls their height.

VII. ESN WITH THE PROPOSED NON-LINEAR ELEMENT AS ACTIVATION FUNCTION

This section describes the substitution of the conventional tanh activation function with the proposed I-V curve, implemented as a custom activation function within an ESN. The ESN was set up using the PyRCN library [41]. To assess the effectiveness of this custom activation function, we utilized the Mackey-Glass time series dataset [42] for predictive modeling. Initially, the baseline parameters for the ESN were established. This was followed by integrating the proposed custom activation function. Prior to its application, the I-V characteristic curve was normalized to serve as an activation function.

Hyperparameter optimization is a critical procedure aimed at enhancing a model's performance by identifying the most effective combination of hyperparameters for a particular dataset. Common strategies for hyperparameter optimization include methods like random search and grid search. The selection of the optimization method is influenced by various factors, including the model's complexity, the breadth of the hyperparameter space, and the computational resources at hand. The overarching aim is to pinpoint an optimal set of hyperparameters efficiently, thereby refining the model's efficacy for the task. The model begins with predetermined parameters, including the size of the hidden layer, the initial activation, bias scaling, and the learning rate. Subsequently, a methodical search is carried out in three step of model training to optimize input scaling, spectral radius, leakage rate, and bias scaling. In the initial step, the input scaling and spectral radius are explored within the ranges of 0.1 to 5 and 0 to 1.5, respectively. Subsequently, a grid search is conducted in the second step to determine the optimal hyperparameter for leakage, examining values from 0 to 1. In the third and final

step, the bias scaling parameter is investigated across a range from 0 to 1.5. The concluding hyperparameters of the ESN, determined through this sequential search, are summarized in Table I.

TABLE I
BEST ESTIMATED ESN HYPERPARAMETERS

Hyperparameter	Value	Hyperparameter	Value
Bias Scaling	1.5	Input Scaling	2
Bias Shift	0	Input Shift	0
Hidden layer size	100	Sparsity	0.1
Spectral Radius	0.6	Leakage	0.5
Learning Rate	1e-5	Bidirectional	False

VIII. Result Analysis and Discussion

Input Mackey-Glass time series signal used to in ESN model with custom activation function. ESN model is trained with 990 time frames and tested with 90 time frames. Each time frame consists of 10 values and in return model predicts the next value of Mackey-Glass time series signal. Predicted time series signal along with the test signal is showed in Fig. 6. The effectiveness of the non-linear activation function is evident from the outcomes presented in the ESN analysis, as delineated in Table II. The effectiveness of our proposed non-linear computation element was assessed using two different performance metrics: the R^2 score and mean squared error. Additionally, its performance was compared with three conventional activation functions: tanh, ReLU, and leaky ReLU. R^2 score or coefficient of determination, serves as a statistical measure that reflects the model's ability to predict unseen signal, with an optimal value of 1. In contrast, mean squared error measures the discrepancy between predicted signal and actual signal, providing a detailed evaluation of an estimator's accuracy, where the optimal value is 0. According to the results presented in the table, although ReLU and leaky ReLU both perform commendably in predicting the Mackey-Glass time series, our proposed function demonstrates a performance comparable to that of the tanh activation function.

This parity underscores the potential of the non-linear element to serve as a viable alternative in neural network applications. Previously, an inkjet printing process was used to implement the hyperbolic sine activation function, which is relatively uncommon, as noted in [38]. However, our inkjet-printed non-linear computation element emulates the more commonly used activation function tanh. Despite experiencing two sharp transitions, this element still functions nearly identical to the traditional tanh activation function.

TABLE II
PERFORMANCE METRIC COMPARISON OF THE ESN WITH DIFFERENT ACTIVATION FUNCTIONS

Activation function	**R^2 Score**	**Mean Squared Error**
ReLU	0.993	1.4×10^{-3}
Leaky ReLU	0.995	1.02×10^{-3}
tanh	0.989	2.52×10^{-3}
Proposed Function	0.986	3.2×10^{-3}

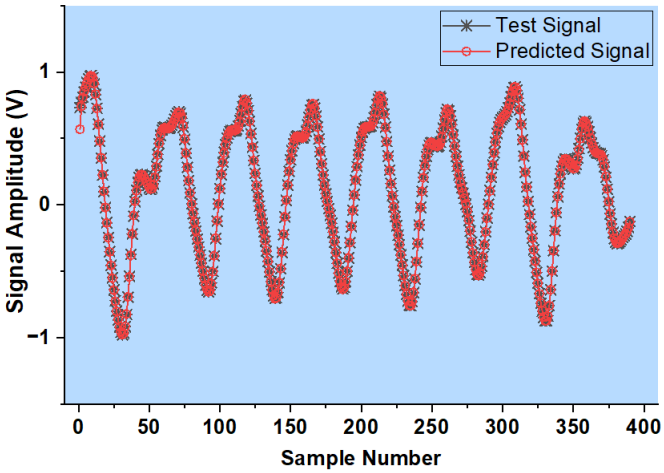

Fig. 6. Test and predicted Mackey-Glass time series signal for ESN network with custom activation function.

IX. Conclusion

This study introduces a novel nonlinear computational element with memristive response in a lower voltage range, created through inkjet printing on a PET film using silver nanoparticle ink. The process is further enhanced by depositing hBN and making precise cuts in the hBN layer to boost the conductivity of the silver nanoparticles. This method produces a nonlinear I-V characteristic curve, making the element suitable as a custom activation function for neural networks. The practicality of using this element as an activation function was tested in an ESN tasked with predicting the benchmark Mackey-Glass time series. The ESN's hyperparameters were optimized through sequential search, with the inkjet-printed nonlinear element serving as the reservoir activation function. The outcomes were compared against traditional activation functions. This research demonstrates that an ESN equipped with an inkjet-printed nonlinear activation element can perform comparably to conventional activation functions while offering benefits futuristic hardware implementation of neural network in terms of lower cost and energy consumption, presenting a potential alternative to standard CMOS technologies.

Acknowledgment

This work was supported by the USA National Science Foundation (NSF) under Grant No. ECCS-2201447. Any opinions, findings, conclusions, or recommendations expressed in this material are those of the author(s) and do not necessarily reflect the views of the National Science Foundation.

References

[1] E. Pritchard, M. Mahfouz, B. Evans, S. Eliza and M. Haider, "Flexible capacitive sensors for high resolution pressure measurement," *SENSORS, 2008 IEEE*, Lecce, Italy, 2008, pp. 1484-1487.

[2] M. R. Haider, S. K. Islam, S. Mostafa, M. Zhang and T. Oh, "Low-Power Low-Voltage Current Readout Circuit for Inductively Powered Implant System," in *IEEE Transactions on Biomedical Circuits and Systems*, vol. 4, no. 4, pp. 205-213, Aug. 2010.

[3] S. K. Islam and M. R. Haider, Sensors and Low Power Signal Processing. New York, NY, USA: Springer, 2010.

[4] M. Zhang, M. R. Haider, M. A. Huque, M. A. Adeeb, S. Rahman, and S. K. Islam, " A low power sensor signal processing circuit for implantable biosensor applications," *Smart Materials and Structures*, vol. 16, no. 2, pp. 525–530.

[5] W. Qu, S. K. Islam, M. R. Mahfouz, M. R. Haider, G. To and S. Mostafa, "Microcantilever Array Pressure Measurement System for Biomedical Instrumentation," in *IEEE Sensors Journal*, vol. 10, no. 2, pp. 321-330, Feb. 2010, doi: 10.1109/JSEN.2009.2034134.

[6] S. Pandey, M. R. Haider, and N. Uddin, "Design and implementation of a low-cost wireless platform for remote bridge health monitoring," *Int. J. Emerg. Technol. Adv. Eng.*, vol. 6, no. 6, pp. 57–62, Jun. 2016.

[7] R. Lu et al., "A Low-Power Sensitive Integrated Sensor System for Thermal Flow Monitoring," in *IEEE Transactions on Very Large Scale Integration (VLSI) Systems*, vol. 27, no. 12, pp. 2949–2953, Dec. 2019.

[8] A.K.M. Arifuzzman, M. R. Haider, and D. B. Allison, "A low-power thermal-based sensor system for low air flow detection," *Analog Integr Circ Sig Process*, 89, 425–436 (2016).

[9] M. A. Adeeb, A. B. Islam, M. R. Haider, F. S. Tulip, M. N. Ericson, S. K. Islam, "An Inductive Link-Based Wireless Power Transfer System for Biomedical Applications", *Active and Passive Electronic Components*, vol. 2012, Article ID 879294, 11 pages, 2012.

[10] Q. Ma, M. R. Haider, S. Yuan and S. K. Islam, "Power-oscillator based high efficiency inductive power-link for transcutaneous power transmission," *2010 53rd IEEE International Midwest Symposium on Circuits and Systems*, Seattle, WA, USA, 2010, pp. 537-540.

[11] Q. Ma, M. R. Haider and S. K. Islam, "A high efficiency inductive power link and backward telemetry for biomedical applications," *SENSORS, 2010 IEEE*, Waikoloa, HI, USA, 2010, pp. 89-93.

[12] A. Khanfor, A. Nammouchi, H. Ghazzai, Y. Yang, M. R. Haider and Y. Massoud, "Graph Neural Networks-based Clustering for Social Internet of Things," *2020 IEEE 63rd International Midwest Symposium on Circuits and Systems (MWSCAS)*, Springfield, MA, USA, 2020, pp. 1056-1059.

[13] A. Khanfor, H. Ghazzai, Y. Yang, M. R. Haider and Y. Massoud, "Automated Service Discovery for Social Internet-of-Things Systems," *2020 IEEE International Symposium on Circuits and Systems (ISCAS)*, Seville, Spain, 2020, pp. 1-5.

[14] P. Ye, T. Ernst, and M. V. Khare, "The last silicon transistor: Nanosheet devices could be the final evolutionary step for Moore's law," *IEEE Spectr.*, vol. 56, no. 8, pp. 30–35, Aug. 2019.

[15] S. Park, M. Vosguerichian, and Z. Bao, "A review of fabrication and applications of carbon nanotube film-based flexible electronics," *Nanoscale*, vol. 5, no. 5, pp. 1727–1752, 2013.

[16] C. Sung, H. Hwang, and I. K. Yoo, "Perspective: A review on memristive hardware for neuromorphic computation," *J. Appl. Phys.*, vol. 124, no. 15, Oct. 2018.

[17] J. Hillier, K. Ibukuro1, L. Liu, M. H. Khaled, J. Byers, and et. al. "Investigating stability and tunability of quantum dot transport in silicon MOSFETs via the application of electrical stress," *J. Phys. D, Appl. Phys.*, vol. 55, no. 10, Dec. 2021.

[18] Z. Dong, D. Qi, Y. He, Z. Xu, X. Hu, and S. Duan, "Easily cascaded memristor-CMOS hybrid circuit for high-efficiency Boolean logic implementation," *Int. J. Bifurcation Chaos*, vol. 28, no. 12, Nov. 2018.

[19] K. Van Pham and K.-S. Min, "Non-ideal effects of memristor-CMOS hybrid circuits for realizing multiple-layer neural networks," in *Proc. IEEE Int. Symp. Circuits Syst. (ISCAS)*, pp. 1–5, May 2019.

[20] G. Liu, L. Zheng, G. Wang, Y. R. Shen, and Y. Liang, "A carry lookahead adder based on hybrid CMOS-memristor logic circuit," *IEEE Access*, vol. 7, pp. 43691–43696, 2019

[21] M. D. Bishop, G. Hills, T. Srimani, D. Murphy, S. Fuller, and et al., "Fabrication of carbon nanotube field-effect transistors in commercial silicon manufacturing facilities," *Nature Electron.*, vol. 3, no. 8, pp. 492–501, Aug. 2020.

[22] Y. Luo, M. Wang, C. Wan, P. Cai, X. J. Loh, and X. Chen, "Devising materials manufacturing toward lab-to-fab translation of flexible electronics," *Adv. Mater.*, vol. 32, no. 37, pp. 2001903, Sep. 2020.

[23] R. Lu, M. R. Haider, S. Gardner, J. I. D. Alexander and Y. Massoud, "A Paper-Based Inkjet-Printed Graphene Sensor for Breathing-Flow Monitoring," in *IEEE Sensors Letters*, vol. 3, no. 2, pp. 1-4, Feb. 2019, Art no. 6000104.

[24] S. D. Gardner, J. I. D. Alexander, Y. Massoud and M. R. Haider, "Minimally produced inkjet-printed tactile sensor model for improved data reliability," *2020 11th International Conference on Electrical and Computer Engineering (ICECE)*, Dhaka, Bangladesh, 2020.

[25] S. D. Gardner, M. R. Haider, M. T. Islam, J. I. D. Alexander and Y. Massoud, "Aluminum-doped Zinc Oxide (ZnO) Inkjet-Printed Piezoelectric Array for Pressure Gradient Mapping," *2019 IEEE 62nd International Midwest Symposium on Circuits and Systems (MWSCAS)*, Dallas, TX, USA, 2019, pp. 1101–1104.

[26] R. F. Hossain and A. B. Kaul, "Inkjet-printed MoS2-based field-effect transistors with graphene and hexagonal boron nitride inks," *J. Vac. Sci. Technol. B*, vol. 38, no. 4, pp. 42206, Jul. 2020.

[27] S. Gardner, A. Porbanderwala and M. R. Haider, "An Affordable Inkjet-Printed Foot Sole Sensor and Machine Learning for Telehealth Devices," *IEEE Sensors Letters*, vol. 7, no. 6, pp. 1-4, June 2023.

[28] S. D. Gardner, J. I. D. Alexander, Y. Massoud and M. R. Haider, "An Inkjet-Printed Paper-Based Flexible Sensor for Pressure Mapping Applications," *2020 IEEE International Symposium on Circuits and Systems (ISCAS)*, Seville, Spain, 2020, pp. 1-5.

[29] S. D. Gardner, M. R. Opu and M. R. Haider, "An Inkjet-Printed Capacitive Sensor for Ultra-Low-Power Proximity and Vibration Detection," *2023 IEEE Wireless and Microwave Technology Conference (WAMICON)*, Melbourne, FL, USA, 2023, pp. 73-76.

[30] F. Wang and T. Arslan, "Inkjet-printed antenna on flexible substrate for wearable microwave imaging applications," *2016 Loughborough Antennas and Propagation Conference (LAPC)*, Loughborough, UK, 2016, pp. 1-4.

[31] Yu H, Zhang X, Zheng H, Li D, Pu Z. "An inkjet-printed bendable antenna for wearable electronics," *Int J Bioprint.* 2023 Mar 29;9(4):722.

[32] H. F. Abutarboush and A. Shamim, "Conformal and green electronics: A wideband inkjet printed antenna on paper substrate," *2013 7th European Conference on Antennas and Propagation (EuCAP)*, Gothenburg, Sweden, 2013, pp. 3099–3102.

[33] S. A. Singaraju, D. D. Weller, T. S. Gspann, J. Aghassi-Hagmann, and M. B. Tahoori, "Artificial Neurons on Flexible Substrates: A Fully Printed Approach for Neuromorphic Sensing," *Sensors*, vol. 22, no. 11, pp. 4000, 2022.

[34] K. J. Yoon, J. Han, J. W. Moon, D. I. Seol, M. L. Meyyappan, M. Kim, and et al., "Electrically-generated memristor based on inkjet printed silver nanoparticles," *Nanoscale Advances*, vol. 1, no. 8, pp. 2990–2998, 2019.

[35] H. Jaeger, "The 'echo state' approach to analysing and training recurrent neural networks-with an erratum note," *German Nat. Res. Center Inf. Technol.*, Karlsruhe, Germany, GMD Tech. Rep. 148, pp. 34, 2001.

[36] Z. Zhao, A. Srivastava, L. Peng, and Q. Chen, "Long short-term memory network design for analog computing," *ACM J. Emerg. Technol. Comput. Syst.*, vol. 15, no. 1, pp. 1–27, Jan. 2019.

[37] W. Maass, T. Natschläger, and H. Markram, "Real-time computing without stable states: A new framework for neural computation based on perturbations," *Neural Comput.*, vol. 14, no. 11, pp. 2531–2560, Nov. 2002.

[38] S. D. Gardner, M. R. Haider, "An inkjet-printed artificial neuron for physical reservoir computing," *IEEE Journal on Flexible Electronics*, vol. 1, no. 3, pp. 185–193, 2022.

[39] G. Tanaka, T. Yamane, J. B. Héroux, R. Nakane, N. Kanazawa, and et al., "Recent advances in physical reservoir computing: A review," *Neural Networks* , vol. 115, pp. 100–123, 2019.

[40] T. Chen, J. van Gelder, B. van de Ven, S. V. Amitonov, B. De Wilde, and et al., "Classification with a disordered dopant-atom network in silicon," *Nature*, vol. 577, no. 7790, pp. 341–345, Jan. 2020.

[41] P. Steiner, A. Jalalvand, S. Stone, and P. Birkholz, "PyRCN: A toolbox for exploration and application of Reservoir Computing Networks," *Engineering Applications of Artificial Intelligence*, vol. 113, pp. 104 964, 2022.

[42] L. Glass, M. Mackey, "Mackey-glass equation," *Scholarpedia*, vol. 5, pp. 6908, 2010.